Supplement of Clim. Past, 16, 1847–1872, 2020
https://doi.org/10.5194/cp-16-1847-2020-supplement

Climate of the Past
Open Access
EGU

Supplement of

Large-scale features and evaluation of the PMIP4-CMIP6 *midHolocene* simulations

Chris M. Brierley et al.

Correspondence to: Chris M. Brierley (c.brierley@ucl.ac.uk)

Table Captions

Table S1

Digital Object Identifier (doi) for each simulation from CMIP6 and CMIP5. Should the hyperlinks in the table not work, the web address can be created manually by adding `https://dx.doi.org/` in front of each doi. The full citations are in the References.

Table S2

Key metrics of change in the PMIP4-CMIP6 *midHolocene* simulations, in either absolute terms or as a percentage of the *piControl* simulations. For comparison with the reconstructions when available, the quoted values are the average simulated at site locations only, otherwise they are area-averages. Northern high-latitude land is defined as any land between 50–80°N. Midcontinental Eurasia is defined as 40–60°N, 30–120°E by Bartlein et al. (2017). Central Asia is defined as 30–50°N, 60–75°E (Christensen et al., 2013) and these values appear in Fig. 12. The northward monsoon expansion is calculated by determining the change in latitude where the zonal mean summer (MJJAS) rain rate (Fig. S1) equals 2 mm/day over the North Africa (15°W–30°E). The area-averaged mean annual rainfall changes are computed over 20°S –0°N, 65–45°W for South America, and 25–30°N, 70–85°E for the Indo-Gangetic Plain. ENSO activity is measured by the change in variance of monthly sea surface temperature anomalies in the Niño3.4 region (5°S–5°N, 170–120°W; Brown et al., 2020). The probability of a 50-year record in which pseudocoral ENSO activity is weak as in reconstructions for 3-5ka BP is shown separately for both the *midHolocene* and *piControl* simulations (Emile-Geay et al., 2016). The zonal sea surface temperature (SST) gradient along the Equatorial Pacific is calculated as difference between the annual mean area average over 5°S–5°N,150–190°E and the annual mean area average over 5°S–5°N,240–270°E after Brown et al. (2020).

Tables S3-S5

Simulated Annual-mean Temperature Changes. The surface air temperature changes averaged in 30° latitude-wide bands are computed for every model included in the study. The allocation of which latitude band a gridbox falls into is determined solely on the gridbox's centroid. Ensemble statistics are also as provided. For the combined ensemble of all models discussed in this manuscript (Tab. S1), we show the mean, maximum, minimum and standard deviation across the ensemble (σ). Only the ensemble mean and standard deviations across the ensemble (σ) are shown for the new (CMIP6/PMIP4) and old (CMIP5/PMIP3) generations of models. A common land-sea mask at $1^\circ \times 1^\circ$ resolution is used for all models (Phillips et al., 2014), which is then converted onto each model's grid.

S3 – Surface Temperature. The proportion of global area contained within each latitude band is provided as 'Areal Fraction'.

S4 – Temperature Change Over Land. The proportion of global land contained within each latitude band is provided as 'Land Fraction'.

S5 – Temperature Change Over Ocean. The proportion of global ocean surface area contained within each latitude band is provided as 'Ocean Fraction'. *The annual mean SST change should closely track the surface air temperature change presented here, but can vary in regions of sea ice cover.*

References

Adler, R. F., Huffman, G. J., Chang, A., Ferraro, R., Xie, P.-P., Janowiak, J., Rudolf, B., Schneider, U., Curtis, S., Bolvin, D., Gruber, A., Susskind, J., Arkin, P., and Nelkin, E.: The version-2 global precipitation climatology project (GPCP) monthly precipitation analysis (1979–present), Journal of hydrometeorology, 4, 1147–1167, https://doi.org/10.1175/1525-7541(2003)004<1147:TVGPCP>2.0.CO;2, 2003.

Bartlein, P. J., Harrison, S., Brewer, S., Connor, S., Davis, B., Gajewski, K., Guiot, J., Harrison-Prentice, T., Henderson, A., and Peyron, O.: Pollen-based continental climate reconstructions at 6 and 21 ka: a global synthesis, Climate Dynamics, 37, 775–802, https://doi.org/10.1007/s00382-010-0904-1, 2011.

Bartlein, P. J., Harrison, S. P., and Izumi, K.: Underlying causes of Eurasian midcontinental aridity in simulations of mid-Holocene climate, Geophysical research letters, 44, 9020–9028, https://doi.org/10.1002/2017GL074476, 2017.

Boucher, O., Denvil, S., Caubel, A., and Foujols, M. A.: IPSL IPSL-CM6A-LR model output prepared for CMIP6 PMIP midHolocene, Earth System Grid Federation, https://doi.org/10.22033/ESGF/CMIP6.5229, 2018a.

Boucher, O., Denvil, S., Caubel, A., and Foujols, M. A.: IPSL IPSL-CM6A-LR model output prepared for CMIP6 CMIP piControl, Earth System Grid Federation, https://doi.org/10.22033/ESGF/CMIP6.5251, 2018b.

Braconnot, P., Otto-Bliesner, B., Harrison, S., Joussaume, S., Peterchmitt, J.-Y., Abe-Ouchi, A., Crucifix, M., Driesschaert, E., Fichefet, T., Hewitt, C., et al.: Results of PMIP2 coupled simulations of the Mid-Holocene and Last Glacial Maximum–Part 1: experiments and large-scale features, Climate of the Past, 3, 261–277, https://doi.org/10.5194/cp-3-261-2007, 2007.

Braconnot, P., Harrison, S. P., Kageyama, M., Bartlein, P. J., Masson-Delmotte, V., Abe-Ouchi, A., Otto-Bliesner, B., and Zhao, Y.: Evaluation of climate models using palaeoclimatic data, Nature Climate Change, 2, 417–424, https://doi.org/10.1038/nclimate1456, 2012.

Brown, J., Brierley, C. M., An, S.-I., Guarino, M.-V., Stevenson, S., Williams, C. J. R., et al.: Comparison of past and future simulations of ENSO in CMIP5/PMIP3 and CMIP6/PMIP4 models, Climate of the Past, https://doi.org/10.5194/cp-2019-155, 2020.

Cao, J.: NUIST NESMv3 model output prepared for CMIP6 PMIP midHolocene, Earth System Grid Federation, https://doi.org/10.22033/ESGF/CMIP6.8773, 2019.

Cao, J. and Wang, B.: NUIST NESMv3 model output prepared for CMIP6 CMIP piControl, Earth System Grid Federation, https://doi.org/10.22033/ESGF/CMIP6.8776, 2019.

Christensen, J., Krishna Kumar, K., Aldrian, E., An, S.-I., Cavalcanti, I., de Castro, M., Dong, W.and Goswami, P., Hall, A., Kanyanga, J., Kitoh, A., Kossin, J., Lau, N.-C., Renwick, J., Stephenson, D., Xie, S.-P., and Zhou, T.: Climate phenomena and their relevance for future regional climate change, in: Climate change 2013: the physical science basis. Contribution of Working Group I to the Fifth Assessment Report of the Intergovernmental Panel on Climate Change, edited by Stocker, T., Qin, D., Plattner, G.-K., Tignor, M., Allen, S., Boschung, J., Nauels, A., Xia, Y., Bex, V., and Midgley, P., pp. 1217–1308, Cambridge University Press, 2013.

Danabasoglu, G.: NCAR CESM2 model output prepared for CMIP6 PMIP midHolocene, Earth System Grid Federation, https://doi.org/10.22033/ESGF/CMIP6.7674, 2019.

Danabasoglu, G., Lawrence, D., Lindsay, K., Lipscomb, W., and Strand, G.: NCAR CESM2 model output prepared for CMIP6 CMIP piControl, Earth System Grid Federation, https://doi.org/10.22033/ESGF/CMIP6.7733, 2019.

Danek, C., Shi, X., Stepanek, C., Yang, H., Barbi, D., Hegewald, J., and Lohmann, G.: AWI AWI-ESM1.1LR model output prepared for CMIP6 CMIP piControl, Earth System Grid Federation, https://doi.org/10.22033/ESGF/CMIP6.9335, 2020.

EC-Earth Consortium (EC-Earth): EC-Earth-Consortium EC-Earth3-LR model output prepared for CMIP6 CMIP piControl, Earth System Grid Federation, https://doi.org/10.22033/ESGF/CMIP6.4847, 2019.

EC-Earth Consortium (EC-Earth): EC-Earth-Consortium EC-Earth3-LR model output prepared for CMIP6 PMIP midHolocene, Earth System Grid Federation, https://doi.org/10.22033/ESGF/CMIP6.4801, 2020.

Emile-Geay, J., Cobb, K. M., Carre, M., Braconnot, P., Leloup, J., Zhou, Y., Harrison, S. P., Correge, T., McGregor, H. V., Collins, M., Driscoll, R., Elliot, M., Schneider, B., and Tudhope, A.: Links between tropical Pacific seasonal, interannual and orbital variability during the Holocene, Nature Geosci, 9, 168–173, https://doi.org/10.1038/ngeo2608, 2016.

Guo, C., Bentsen, M., Bethke, I., Ilicak, M., Tjiputra, J., Toniazzo, T., Schwinger, J., and Otterå, O. H.: NCC NorESM1-F model output prepared for CMIP6 PMIP midHolocene, Earth System Grid Federation, https://doi.org/10.22033/ESGF/CMIP6.11591, 2019a.

Guo, C., Bentsen, M., Bethke, I., Ilicak, M., Tjiputra, J., Toniazzo, T., Schwinger, J., and Otterå, O. H.: NCC NorESM1-F model output prepared for CMIP6 CMIP piControl, Earth System Grid Federation, https://doi.org/10.22033/ESGF/CMIP6.11595, 2019b.

Hajima, T., Abe, M., Arakawa, O., Suzuki, T., Komuro, Y., Ogura, T., Ogochi, K., Watanabe, M., Yamamoto, A., Tatebe, H., Noguchi, M. A., Ohgaito, R., Ito, A., Yamazaki, D., Ito, A., Takata, K., Watanabe, S., Kawamiya, M., and Tachiiri, K.: MIROC MIROC-ES2L model output prepared for CMIP6 CMIP piControl, Earth System Grid Federation, https://doi.org/10.22033/ESGF/CMIP6.5710, 2019.

Hargreaves, J. C., Annan, J. D., Ohgaito, R., Paul, A., and Abe-Ouchi, A.: Skill and reliability of climate model ensembles at the Last Glacial Maximum and mid-Holocene, Climate of the Past, 9, 811–823, https://doi.org/10.5194/cp-9-811-2013, 2013.

Joussaume, S., Taylor, K. E., Braconnot, P., Mitchell, J. F. B., Kutzbach, J. E., Harrison, S. P., Prentice, I. C., Broccoli, A. J., Abe-Ouchi, A., Bartlein, P. J., Bonfils, C., Dong, B., Guiot, J., Herterich, K., Hewitt, C. D., Jolly, D., Kim, J. W., Kislov, A., Kitoh, A., Loutre, M. F., Masson, V., McAvaney, B., McFarlane, N., de Noblet, N., Peltier, W. R., Peterschmitt, J. Y., Pollard, D., Rind, D., Royer, J. F., Schlesinger, M. E., Syktus, J., Thompson, S., Valdes, P., Vettoretti, G., Webb, R. S., and Wyputta, U.: Monsoon changes for 6000 years ago: results of 18 simulations from the Paleoclimate Modeling Intercomparison Project (PMIP), Geophysical Research Letters, 26, 859–862, https://doi.org/10.1029/1999GL900126, 1999.

Kaufman, D., McKay, N., Routson, C., Erb, M., Dätwyler, C., Sommer, P., Heiri, O., and Davis, B.: Holocene global mean surface temperature: a multi-method reconstruction approach, Scientific Data, 7, 1–13, https://doi.org/10.1038/s41597-020-0530-7, 2020a.

Kaufman, D., McKay, N., Routson, C., Erb, M., Davis, B., Heiri, O., Jaccard, S., Tierney, J., Dätwyler, C., Axford, Y., Brussel, T., Cartapanis, O., Chase, B., Dawson, A., de Vernal, A., Engels, S., Jonkers, L., Marsicek, J., Moffa-Sánchez, P., Morrill, C., Orsi, A., Rehfeld, K., Saunders, K., Sommer, P. S., Thomas, E., Tonello, M., Tóth, M., Vachula, R., Andreev, A., Bertrand, S., Biskaborn, B., Bringué, M., Brooks, S., Caniupán, M., Chevalier, M., Cwynar, L., Emile-Geay, J., Fegyveresi, J., Feurdean, A., Finsinger, W., Fortin, M.-C., Foster, L., Fox, M., Gajewski, K., Grosjean, M., Hausmann, S., Heinrichs, M., Holmes, N., Ilyashuk, B., Ilyashuk, E., Juggins, S., Khider, D., Koinig, K., Langdon, P., Larocque-Tobler, I., Li, J., Lotter, A., Luoto, T., Mackay, A., Magyari, E., Malevich, S., Mark, B., Massaferro, J., Montade, V., Nazarova, L., Novenko, E., Pařil, P., Pearson, E., Peros, M., Pienitz, R., Płóciennik, M., Porinchu, D., Potito, A., Rees, A., Reinemann, S., Roberts, S., Rolland, N., Salonen, S., Self, A., Sepp a, H., Shala, S., St-Jacques, J.-M., Stenni, B., Syrykh, L., Tarrats, P., Taylor, K., van den Bos, V., Velle, G., Wahl, E., Walker, I., Wilmshurst, J., Zhang, E., and Zhilich, S.: A global database of Holocene paleo-temperature records, Scientific Data, 7, 115, https://doi.org/10.1038/s41597-020-0445-3, 2020b.

Li, L.: CAS FGOALS-g3 model output prepared for CMIP6 CMIP piControl, Earth System Grid Federation, https://doi.org/10.22033/ESGF/CMIP6.3448, 2019.

NASA Goddard Institute for Space Studies (NASA/GISS): NASA-GISS GISS-E2.1G model output prepared for CMIP6 CMIP piControl, Earth System Grid Federation, https://doi.org/10.22033/ESGF/CMIP6.7380, 2018.

NASA Goddard Institute for Space Studies (NASA/GISS): NASA-GISS GISS-E2.1G model output prepared for CMIP6 PMIP midHolocene, Earth System Grid Federation, https://doi.org/10.22033/ESGF/CMIP6.7225, 2019.

New, M., Hulme, M., and Jones, P.: Representing twentieth-century space–time climate variability. Part II: Development of 1901–96 monthly grids of terrestrial surface climate, Journal of Climate, 13, 2217–2238, https://doi.org/10.1175/1520-0442(2000)013<2217:RTCSTC>2.0.CO;2, 2000.

Ohgaito, R., Abe-Ouchi, A., Abe, M., Arakawa, O., Ogochi, K., Hajima, T., Watanabe, M., Yamamoto, A., Tatebe, H., Noguchi, M. A., Ito, A., Yamazaki, D., Ito, A., Takata, K., Watanabe, S., Kawamiya, M., and Tachiiri, K.: MIROC MIROC-ES2L model output prepared for CMIP6 PMIP midHolocene, Earth System Grid Federation, https://doi.org/10.22033/ESGF/CMIP6.5646, 2019.

Phillips, A. S., Deser, C., and Fasullo, J.: Evaluating modes of variability in climate models, Eos, Transactions American Geophysical Union, 95, 453–455, https://doi.org/10.1002/2014EO490002, 2014.

Ridley, J., Menary, M., Kuhlbrodt, T., Andrews, M., and Andrews, T.: MOHC HadGEM3-GC31-LL model output prepared for CMIP6 CMIP piControl, Earth System Grid Federation, https://doi.org/10.22033/ESGF/CMIP6.6294, 2018.

Seland, o., Bentsen, M., Oliviè, D. J. L., Toniazzo, T., Gjermundsen, A., Graff, L. S., Debernard, J. B., Gupta, A. K., He, Y., Kirkevåg, A., Schwinger, J., Tjiputra, J., Aas, K. S., Bethke, I., Fan, Y., Griesfeller, J., Grini, A., Guo, C., Ilicak, M., Karset, I. H. H., Landgren, O. A., Liakka, J., Moseid, K. O., Nummelin, A., Spensberger, C., Tang, H., Zhang, Z., Heinze, C., Iversen, T., and Schulz, M.: NCC NorESM2-LM model output prepared for CMIP6 CMIP piControl, Earth System Grid Federation, https://doi.org/10.22033/ESGF/CMIP6.8217, 2019.

Shi, X., Yang, H., Danek, C., and Lohmann, G.: AWI AWI-ESM1.1LR model output prepared for CMIP6 PMIP midHolocene, Earth System Grid Federation, https://doi.org/10.22033/ESGF/CMIP6.9332, 2020.

Taylor, K. E.: Summarizing multiple aspects of model performance in a single diagram, Journal of Geophysical Research: Atmospheres, 106, 7183–7192, https://doi.org/10.1029/2000JD900719, 2001.

Volodin, E., Mortikov, E., Gritsun, A., Lykossov, V., Galin, V., Diansky, N., Gusev, A., Kostrykin, S., Iakovlev, N., Shestakova, A., and Emelina, S.: INM INM-CM4-8 model output prepared for CMIP6 PMIP midHolocene, Earth System Grid Federation, https://doi.org/10.22033/ESGF/CMIP6.5077, 2019a.

Volodin, E., Mortikov, E., Gritsun, A., Lykossov, V., Galin, V., Diansky, N., Gusev, A., Kostrykin, S., Iakovlev, N., Shestakova, A., and Emelina, S.: INM INM-CM4-8 model output prepared for CMIP6 CMIP piControl, Earth System Grid Federation, https://doi.org/10.22033/ESGF/CMIP6.5080, 2019b.

Xie, P. and Arkin, P. A.: Global precipitation: A 17-year monthly analysis based on gauge observations, satellite estimates, and numerical model outputs, Bulletin of the American Meteorological Society, 78, 2539–2558, https://doi.org/10.1175/2008JAMC1921.1, 1997.

Yu, Y.: CAS FGOALS-f3-L model output prepared for CMIP6 CMIP piControl, Earth System Grid Federation, https://doi.org/10.22033/ESGF/CMIP6.3447, 2019.

Yukimoto, S., Koshiro, T., Kawai, H., Oshima, N., Yoshida, K., Urakawa, S., Tsujino, H., Deushi, M., Tanaka, T., Hosaka, M., Yoshimura, H., Shindo, E., Mizuta, R., Ishii, M., Obata, A., and Adachi, Y.: MRI MRI-ESM2.0 model output prepared for CMIP6 PMIP midHolocene, Earth System Grid Federation, https://doi.org/10.22033/ESGF/CMIP6.6860, 2019a.

Yukimoto, S., Koshiro, T., Kawai, H., Oshima, N., Yoshida, K., Urakawa, S., Tsujino, H., Deushi, M., Tanaka, T., Hosaka, M., Yoshimura, H., Shindo, E., Mizuta, R., Ishii, M., Obata, A., and Adachi, Y.: MRI MRI-ESM2.0 model output prepared for CMIP6 CMIP piControl, Earth System Grid Federation, https://doi.org/10.22033/ESGF/CMIP6.6900, 2019b.

Zhang, Z., Bentsen, M., Oliviè, D. J. L., Seland, o., Toniazzo, T., Gjermundsen, A., Graff, L. S., Debernard, J. B., Gupta, A. K., He, Y., Kirkevåg, A., Schwinger, J., Tjiputra, J., Aas, K. S., Bethke, I., Fan, Y., Griesfeller, J., Grini, A., Guo, C., Ilicak, M., Karset, I. H. H., Landgren, O. A., Liakka, J., Moseid, K. O., Nummelin, A., Spensberger, C., Tang, H., Heinze, C., Iversen, T., and Schulz, M.: NCC NorESM2-LM model output prepared for CMIP6 PMIP midHolocene, Earth System Grid Federation, https://doi.org/10.22033/ESGF/CMIP6.8079, 2019.

Zheng, W. and Dong, L.: CAS FGOALS-g3 model output prepared for CMIP6 PMIP midHolocene, Earth System Grid Federation, https://doi.org/10.22033/ESGF/CMIP6.3409, 2019.

Zheng, W. and He, B.: CAS FGOALS-f3-L model output prepared for CMIP6 PMIP midHolocene, Earth System Grid Federation, https://doi.org/10.22033/ESGF/CMIP6.12014, 2019.

Table S1. Digital Object Identifier (doi) for each simulation from CMIP6 and CMIP5. Should the hyperlinks in the table not work, the web address can be created manually by adding `https://dx.doi.org/` in front of each doi. The full citations are in the References.

model	*midHolocene*	*piControl*
AWI-ESM-1-1-LR	10.22033/ESGF/CMIP6.9332	10.22033/ESGF/CMIP6.9335
CESM2	10.22033/ESGF/CMIP6.7674	10.22033/ESGF/CMIP6.7733
EC-Earth3-LR	10.22033/ESGF/CMIP6.4847	10.22033/ESGF/CMIP6.4801
FGOALS-f3-L	10.22033/ESGF/CMIP6.12014	10.22033/ESGF/CMIP6.3447
FGOALS-g3	10.22033/ESGF/CMIP6.3409	10.22033/ESGF/CMIP6.3448
GISS-E2-1-G	10.22033/ESGF/CMIP6.7225	10.22033/ESGF/CMIP6.7380
HadGEM3-GC31-LL	N/A	10.22033/ESGF/CMIP6.6294
INM-CM4-8	10.22033/ESGF/CMIP6.5077	10.22033/ESGF/CMIP6.5080
IPSL-CM6A-LR	10.22033/ESGF/CMIP6.5229	10.22033/ESGF/CMIP6.5251
MIROC-ES2L	10.22033/ESGF/CMIP6.5646	10.22033/ESGF/CMIP6.5710
MRI-ESM2	10.22033/ESGF/CMIP6.6860	10.22033/ESGF/CMIP6.6900
NESM3	10.22033/ESGF/CMIP6.8773	10.22033/ESGF/CMIP6.8776
NorESM1-F	10.22033/ESGF/CMIP6.11591	10.22033/ESGF/CMIP6.11595
NorESM2-LM	10.22033/ESGF/CMIP6.8079	10.22033/ESGF/CMIP6.8217
UofT-CCSM-4	N/A	N/A
bcc-csm1-1	10.1594/WDCC/CMIP5.BCB1mh	10.1594/WDCC/CMIP5.BCB1pc
CCSM4	10.1594/WDCC/CMIP5.NRS4mh	10.1594/WDCC/CMIP5.NRS4pc
CNRM-CM5	10.1594/WDCC/CMIP5.CEC5mh	10.1594/WDCC/CMIP5.CEC5pc
CSIRO-MK3-6-0	10.1594/WDCC/CMIP5.CQMKmh	10.1594/WDCC/CMIP5.CQMKpc
CSIRO-MK3L-1-2	N/A	N/A
EC-Earth-2-2	N/A	N/A
FGOALS-G2	10.1594/WDCC/CMIP5.LSF2mh	10.1594/WDCC/CMIP5.LSF2pc
FGOALS-S2	10.1594/WDCC/CMIP5.LIFSmh	10.1594/WDCC/CMIP5.LIFSpc
GISS-E2-R	10.1594/WDCC/CMIP5.GIGRmh	10.1594/WDCC/CMIP5.GIGRpc
HadGEM2-CC	10.1594/WDCC/CMIP5.MOGCmh	10.1594/WDCC/CMIP5.MOGCpc
HadGEM2-ES	10.1594/WDCC/CMIP5.MOGEmh	10.1594/WDCC/CMIP5.MOGEpc
IPSL-CM5A-LR	10.1594/WDCC/CMIP5.IPILmh	10.1594/WDCC/CMIP5.IPILpc
MIROC-ESM	10.1594/WDCC/CMIP5.MIMEmh	10.1594/WDCC/CMIP5.MIMEpc
MPI-ESM-P	10.1594/WDCC/CMIP5.MXEPmh	10.1594/WDCC/CMIP5.MXEPpc
MRI-CGCM3	10.1594/WDCC/CMIP5.MRMCmh	10.1594/WDCC/CMIP5.MRMCpc

N/A indicates that a doi is not available.

Table S2. Key metrics of change in the PMIP4-CMIP6 *midHolocene* simulations see above for further details

	Extratropical						Tropical						
	Global mean temperature (°C)	Summer NH high-lat. land (°C)	Drier Eastern North America (mm/yr)	Midcontinental Eurasia rainfall (mm/yr)	Midcontinental Eurasia Seasonality (°C)	Central Asian Seasonality (°C)	N. African monsoon expansion (°N)	Drier South America (mm/yr)	Indo-Gangetic rainfall (mm/yr)	Niño3.4 Variance‡ (%)	p(suppressed ENSO) in *piControl*§ (%)	p(suppressed ENSO) in *midHolocene*§ (%)	Eq. Pac SST gradient‡ (%)
AWI-ESM-1-1-LR	-0.4	0.0	-58	-21	2.6	2.9	3.1	68	115	-41	–	–	-8
CESM2	-0.2	0.7	-54	-16	2.8	3.1	-0.2	-97	125	-16	2.4	5.7	-7
EC-Earth3-LR	-0.1	1.8	-28	12	2.3	2.3	-0.5	-29	166	-31	–	–	-5
FGOALS-f3-L	-0.4	0.6	-24	-11	3.0	3.0	1.5	-85	165	4	2.8	1.2	0
FGOALS-g3	-0.2	1.1	-92	-58	4.2	4.1	1.8	-258	57	-14	0.2	2.5	-1
GISS-E2-1-G	-0.4	0.7	-15	-9	2.4	2.6	1.6	-60	188	2	1.8	5.6	4
HadGEM3-GC31-LL	-0.1	1.2	-9	2	3.0	3.8	2.3	-102	207	-8	0.6	0.6	-3
INM-CM4-8	-0.3	0.7	24	-2	2.7	3.1	2.1	-96	212	7	1.5	14.2	-4
IPSL-CM6A-LR	-0.4	0.5	-23	-32	3.5	3.0	0.9	-72	160	-13	1.7	3.4	-3
MIROC-ES2L	-0.5	0.6	30	-26	2.8	3.4	1.3	-111	77	-49	7.3	82.4	16
MPI-ESM1-2-LR	-0.4	0.6	-26	-18	2.8	3.0	3.7	-179	189	-28	1.1	7.4	-4
MRI-ESM2-0	-0.2	0.7	-22	-15	2.5	2.7	3.3	-179	189	-36	4.8	34.5	0
NESM3	-0.3	0.9	59	24	2.6	2.5	3.1	-155	177	-24	2.1	5.2	-4
NorESM1-F	-0.4	0.4	-6	-8	3.4	3.6	1.4	-116	158	-6	–	–	-6
NorESM2-LM	-0.2	0.5	137	137	3.3	3.0	-1.9	-85	255	11	–	–	-8
UofT-CCSM-4	-0.2	1.1	-8	-3	3.1	2.8	1.9	-117	114	-48	–	–	-2
Reconstructed	0.5†	0.7*	-93¶	121¶	–	–	–	–	–	–	–	–	–
PMIP4 Average	-0.3	0.8	-7	-3	2.9	3.1	1.7	-99	162	-18	2.4	14.8	-1.9
PMIP3 Average	-0.1	1.	-10	-4	2.6	2.9	3.0	-83	175	-11	3.7§	5.8§	-3
PMIP3 Spread	0.2	0.5	19	15	0.4	0.4	4.2	46	81	14	3.2§	4.3§	6

†Median reconstructed global mean value from Kaufman et al. (2020a), with 80% confidence interval of 0.3–0.9 °C. *average of the difference in summer and winter reconstructions within the region from Kaufman et al. (2020b) compilation. ¶average of reconstructions within the region from Bartlein et al. (2011) compilation. ‡Values published in Brown et al. (2020). §Using the analysis approach of Emile-Geay et al. (2016) with PMIP3 values directly from it.

Table S3. Annual mean surface air temperature change see above for further details

	Global	60°N–90°N	30°N–60°N	0°–30°N	30°S–0°	60°S–30°S	90°S–60°S
Areal Fraction	1	0.067	0.183	0.25	0.25	0.183	0.067
AWI-ESM-1-1-LR	-0.44	-0.62	-0.47	-0.69	-0.49	-0.18	0.23
CESM2	-0.21	0.14	-0.09	-0.41	-0.3	-0.13	0.08
EC-Earth3-LR	-0.05	1.3	0.26	-0.34	-0.26	-0.19	0.05
FGOALS-f3-L	-0.37	-0.04	-0.38	-0.54	-0.39	-0.26	-0.25
FGOALS-g3	-0.23	0.22	-0.02	-0.51	-0.26	-0.16	-0.08
GISS-E2-1-G	-0.38	0.43	-0.27	-0.59	-0.41	-0.41	-0.54
HadGEM3-GC31-LL	-0.13	0.79	0.08	-0.4	-0.37	-0.13	0.33
INM-CM4-8	-0.3	-0.04	-0.36	-0.43	-0.3	-0.21	-0.14
IPSL-CM6A-LR	-0.36	-0.25	-0.31	-0.53	-0.43	-0.24	-0.08
MIROC-ES2L	-0.47	-0.15	-0.45	-0.66	-0.49	-0.34	-0.43
MPI-ESM1-2-LR	-0.36	-0.13	-0.35	-0.67	-0.37	-0.16	0.02
MRI-ESM2-0	-0.18	0.18	0.03	-0.49	-0.35	-0.04	0.36
NESM3	-0.27	0.17	-0.44	-0.54	-0.19	-0.09	-0.01
NorESM1-F	-0.36	-0.33	-0.43	-0.47	-0.3	-0.31	-0.18
NorESM2-LM	-0.22	0.03	-0.09	-0.32	-0.33	-0.2	-0.03
UofT-CCSM-4	-0.17	0.61	-0.18	-0.45	-0.24	-0.07	0.23
BCC-CSM1-1	-0.14	0.86	-0.01	-0.4	-0.29	-0.08	0.05
CCSM4	-0.26	-0.07	-0.36	-0.45	-0.22	-0.11	-0.03
CNRM-CM5	0.18	1.36	0.34	-0.07	-0.03	0.11	0.47
CSIRO-Mk3-6-0	0.02	0.4	0.15	-0.21	-0.18	0.11	0.59
CSIRO-Mk3L-1-2	-0.01	0.58	0.21	-0.24	-0.2	-0.03	0.41
EC-EARTH-2-2	-0.11	0.8	0.09	-0.44	-0.21	-0.05	0.01
FGOALS-g2	-0.73	-0.64	-0.64	-0.94	-0.77	-0.55	-0.63
FGOALS-s2	-0.16	0.41	-0.11	-0.43	-0.32	-0.04	0.32
GISS-E2-R	-0.1	0.73	0.02	-0.43	-0.29	-0.09	0.68
HadGEM2-CC	0.22	1.67	0.46	-0.07	-0.09	0.1	0.6
HadGEM2-ES	0.24	1.27	0.54	0.01	-0.03	0.07	0.71
IPSL-CM5A-LR	-0.09	0.34	0.2	-0.28	-0.25	-0.15	0.19
MIROC-ESM	-0.25	-0.28	-0.29	-0.59	-0.37	0.07	0.83
MPI-ESM-P	-0.24	0.17	-0.08	-0.54	-0.35	-0.14	0.16
MRI-CGCM3	-0.02	0.78	0.15	-0.27	-0.23	0.02	0.32
Combined Mean	-0.19	0.34	-0.09	-0.43	-0.3	-0.13	0.14
Combined Max	0.24	1.67	0.54	0.01	-0.03	0.11	0.83
Combined Min	-0.73	-0.64	-0.64	-0.94	-0.77	-0.55	-0.63
Combined σ	0.21	0.58	0.3	0.2	0.14	0.15	0.36
CMIP6/PMIP4 Mean	-0.27	0.19	-0.2	-0.5	-0.34	-0.19	-0.02
CMIP6/PMIP4 σ	0.12	0.48	0.22	0.11	0.08	0.1	0.24
CMIP5/PMIP3 Mean	-0.09	0.54	0.05	-0.35	-0.25	-0.05	0.33
CMIP5/PMIP3 σ	0.25	0.64	0.32	0.25	0.18	0.17	0.38

Table S4. Land surface air temperature change see above for further details

	Global	60°N–90°N	30°N–60°N	0°–30°N	30°S–0°	60°S–30°S	90°S–60°S
Land Fraction	1	0.118	0.312	0.247	0.196	0.037	0.09
AWI-ESM-1-1-LR	-0.63	-0.56	-0.44	-1.25	-0.57	-0.34	0.09
CESM2	-0.22	-0.02	-0.08	-0.66	-0.15	-0.12	0.06
EC-Earth3-LR	-0.08	0.84	0.15	-0.69	-0.16	-0.11	-0.13
FGOALS-f3-L	-0.46	-0.19	-0.42	-0.86	-0.36	-0.33	-0.16
FGOALS-g3	-0.04	0.24	0.1	-0.52	0.2	-0.01	-0.05
GISS-E2-1-G	-0.45	0.28	-0.28	-1	-0.4	-0.37	-0.57
HadGEM3-GC31-LL	-0.2	0.35	-0.02	-0.74	-0.31	-0.24	0.15
INM-CM4-8	-0.39	-0.23	-0.47	-0.68	-0.19	-0.27	-0.07
IPSL-CM6A-LR	-0.44	-0.38	-0.35	-0.8	-0.37	-0.33	-0.08
MIROC-ES2L	-0.6	-0.26	-0.54	-1.03	-0.45	-0.43	-0.35
MPI-ESM1-2-LR	-0.51	-0.22	-0.34	-1.26	-0.28	-0.13	-0.09
MRI-ESM2-0	-0.26	0.07	-0.04	-0.82	-0.26	-0.16	0.1
NESM3	-0.4	-0.03	-0.44	-1.03	-0.02	-0.07	0.05
NorESM1-F	-0.5	-0.47	-0.51	-0.81	-0.27	-0.28	-0.22
NorESM2-LM	-0.19	-0.06	-0.09	-0.47	-0.16	-0.22	0.04
UofT-CCSM-4	-0.24	0.36	-0.28	-0.74	-0.06	-0.07	0.05
BCC-CSM1-1	-0.17	0.59	-0.02	-0.66	-0.28	-0.14	0.07
CCSM4	-0.41	-0.25	-0.4	-0.82	-0.25	-0.12	0.03
CNRM-CM5	0.21	0.92	0.32	-0.27	0.12	0.14	0.4
CSIRO-Mk3-6-0	0	0.26	0.21	-0.5	-0.18	0.03	0.62
CSIRO-Mk3L-1-2	0.01	0.45	0.19	-0.51	-0.09	-0.08	0.38
EC-EARTH-2-2	-0.14	0.66	0.05	-0.92	-0.08	-0.07	0.2
FGOALS-g2	-0.85	-0.69	-0.65	-1.32	-0.82	-0.56	-0.46
FGOALS-s2	-0.26	0.23	-0.15	-0.8	-0.24	-0.11	0.07
GISS-E2-R	-0.18	0.34	-0.11	-0.71	-0.18	-0.15	0.36
HadGEM2-CC	0.25	1.17	0.43	-0.3	0.05	0.06	0.53
HadGEM2-ES	0.34	0.89	0.57	-0.19	0.18	0.09	0.71
IPSL-CM5A-LR	-0.06	0.23	0.16	-0.44	-0.16	-0.23	0.17
MIROC-ESM	-0.42	-0.22	-0.36	-0.95	-0.34	-0.28	0.44
MPI-ESM-P	-0.32	0.02	-0.05	-1.02	-0.28	-0.18	0.06
MRI-CGCM3	-0.06	0.5	0.12	-0.54	-0.19	-0.08	0.22
Combined Mean	-0.25	0.16	-0.12	-0.75	-0.21	-0.17	0.08
Combined Max.	0.34	1.17	0.57	-0.19	0.2	0.14	0.71
Combined Min	-0.85	-0.69	-0.65	-1.32	-0.82	-0.56	-0.57
Combined σ	0.26	0.46	0.31	0.28	0.21	0.16	0.29
CMIP6/PMIP4 Mean	-0.34	0.02	-0.24	-0.82	-0.24	-0.21	-0.07
CMIP6/PMIP4 σ	0.18	0.38	0.22	0.23	0.18	0.12	0.18
CMIP5/PMIP3 Mean	-0.14	0.32	0.02	-0.66	-0.18	-0.11	0.27
CMIP5/PMIP3 σ	0.31	0.51	0.34	0.33	0.24	0.18	0.3

Table S5. Annual mean surface air temperature change over the ocean see above for further details

	Global	60°N–90°N	30°N–60°N	0°–30°N	30°S–0°	60°S–30°S	90°S–60°S
Ocean Fraction	1	0.045	0.129	0.251	0.273	0.244	0.057
AWI-ESM-1-1-LR	-0.36	-0.68	-0.5	-0.45	-0.47	-0.18	0.32
CESM2	-0.2	0.3	-0.1	-0.3	-0.34	-0.14	0.09
EC-Earth3-LR	-0.04	1.79	0.37	-0.19	-0.3	-0.2	0.17
FGOALS-f3-L	-0.33	0.13	-0.33	-0.41	-0.4	-0.26	-0.31
FGOALS-g3	-0.3	0.2	-0.13	-0.5	-0.4	-0.17	-0.09
GISS-E2-1-G	-0.35	0.58	-0.25	-0.41	-0.41	-0.42	-0.52
HadGEM3-GC31-LL	-0.1	1.28	0.19	-0.27	-0.38	-0.12	0.44
INM-CM4-8	-0.26	0.16	-0.25	-0.33	-0.33	-0.21	-0.18
IPSL-CM6A-LR	-0.33	-0.11	-0.26	-0.42	-0.45	-0.23	-0.08
MIROC-ES2L	-0.42	-0.04	-0.36	-0.51	-0.5	-0.33	-0.49
MPI-ESM1-2-LR	-0.3	-0.02	-0.35	-0.43	-0.4	-0.16	0.09
MRI-ESM2-0	-0.14	0.3	0.11	-0.35	-0.38	-0.04	0.54
NESM3	-0.21	0.41	-0.43	-0.33	-0.24	-0.09	-0.06
NorESM1-F	-0.3	-0.18	-0.35	-0.33	-0.31	-0.31	-0.15
NorESM2-LM	-0.23	0.11	-0.08	-0.25	-0.39	-0.2	-0.09
UofT-CCSM-4	-0.13	0.88	-0.08	-0.33	-0.29	-0.07	0.35
BCC-CSM1-1	-0.12	1.15	0	-0.28	-0.29	-0.08	0.03
CCSM4	-0.2	0.12	-0.32	-0.3	-0.21	-0.11	-0.07
CNRM-CM5	0.17	1.83	0.35	0	-0.07	0.11	0.52
CSIRO-Mk3-6-0	0.02	0.56	0.08	-0.09	-0.19	0.11	0.57
CSIRO-Mk3L-1-2	-0.01	0.72	0.23	-0.14	-0.23	-0.02	0.43
EC-EARTH-2-2	-0.09	0.96	0.12	-0.24	-0.25	-0.05	-0.12
FGOALS-g2	-0.68	-0.57	-0.62	-0.78	-0.75	-0.54	-0.72
FGOALS-s2	-0.12	0.62	-0.06	-0.27	-0.35	-0.04	0.47
GISS-E2-R	-0.07	1.15	0.15	-0.32	-0.33	-0.09	0.87
HadGEM2-CC	0.2	2.24	0.48	0.03	-0.13	0.1	0.64
HadGEM2-ES	0.2	1.7	0.51	0.09	-0.1	0.07	0.7
IPSL-CM5A-LR	-0.1	0.46	0.24	-0.21	-0.27	-0.14	0.21
MIROC-ESM	-0.18	-0.35	-0.22	-0.43	-0.38	0.09	1.12
MPI-ESM-P	-0.21	0.33	-0.12	-0.34	-0.36	-0.14	0.23
MRI-CGCM3	-0.01	1.07	0.18	-0.16	-0.24	0.02	0.39
Combined Mean	-0.17	0.55	-0.06	-0.3	-0.33	-0.12	0.17
Combined Max.	0.2	2.24	0.51	0.09	-0.07	0.11	1.12
Combined Min	-0.68	-0.68	-0.62	-0.78	-0.75	-0.54	-0.72
Combined σ	0.19	0.72	0.29	0.17	0.13	0.15	0.42
CMIP6/PMIP4 Mean	-0.24	0.37	-0.16	-0.36	-0.37	-0.19	0
CMIP6/PMIP4 σ	0.11	0.61	0.23	0.09	0.07	0.1	0.3
CMIP5/PMIP3 Mean	-0.08	0.77	0.07	-0.23	-0.28	-0.05	0.37
CMIP5/PMIP3 σ	0.22	0.8	0.31	0.22	0.17	0.17	0.46

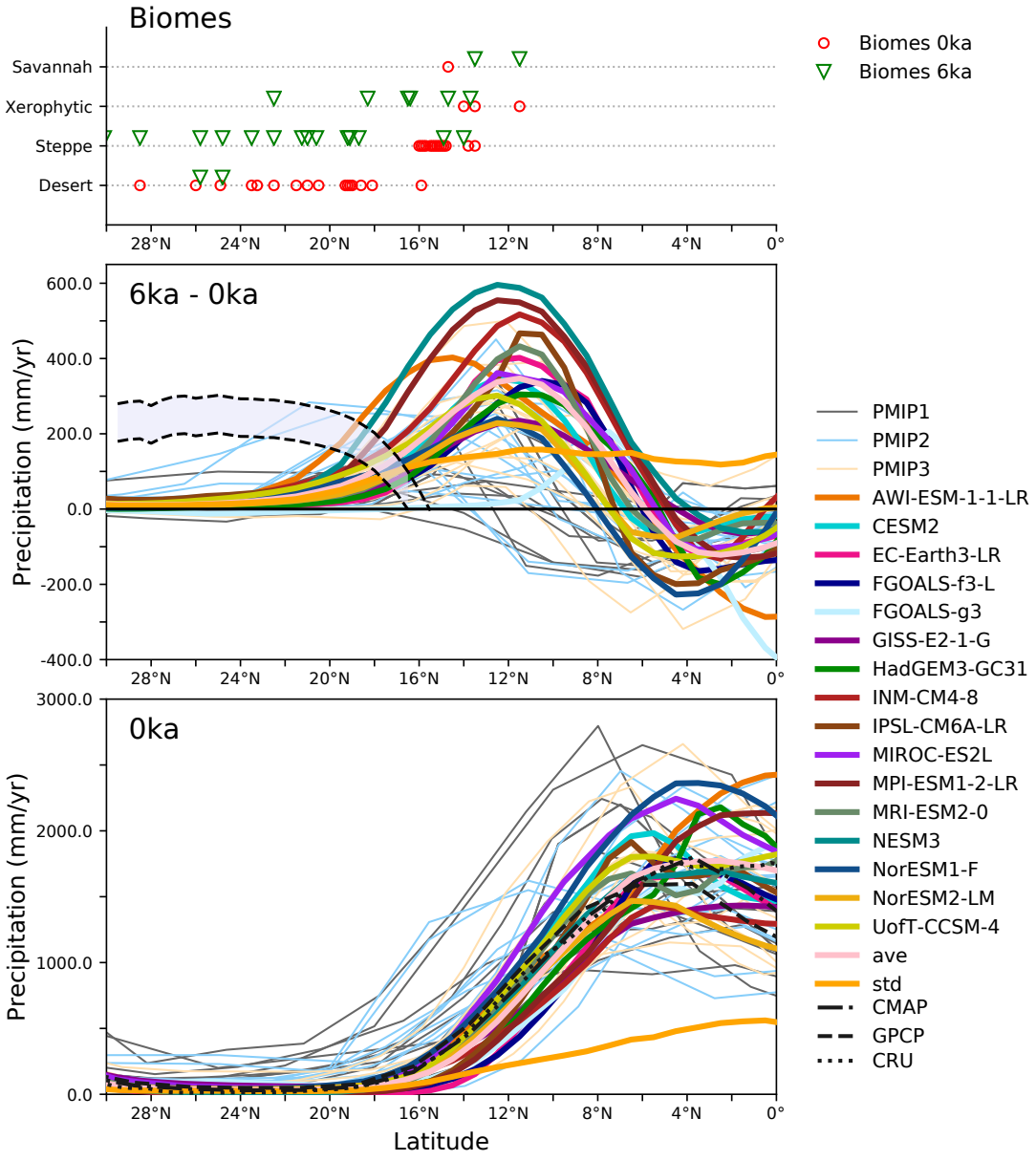

Figure S1. Simulated North African monsoon through multiple phases of PMIP-CMIP. (top panel) Biome distributions (desert, steppe, xerophytic and savannah/dry tropical forest) as a function of latitude for present (red circles) and 6 ka (green triangles), showing that steppe vegetation replaces desert at 6 ka as far north as 23°N (middle panel) Annual mean precipitation changes (mm/yr) over Africa (20°W–30°E) for the Mid-Holocene climate across multiple PMIP generations. The black hatched lines are estimated upper and lower bounds for the additional precipitation required to support steppe at each latitude during the mid-Holocene based on water-balance modelling and the modern climatic requirements for desert and grassland plants. (bottom panel) The rainfall distribution in piControl simulations for each model. Three different observationally-based datasets are shown in black: GPCP (Adler et al., 2003), CMAP (Xie and Arkin, 1997), and CRU (New et al., 2000). (Adapted from Joussaume et al., 1999; Braconnot et al., 2007, 2012)

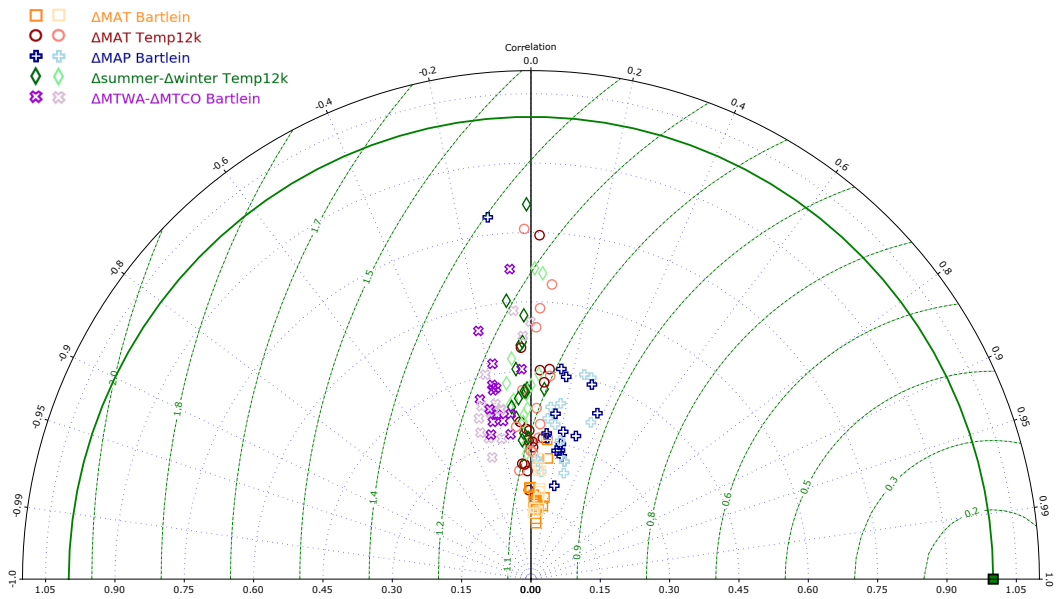

Figure S2. Statistical description of site-level comparison of simulated mid-Holocene climate changes to reconstructions. The performance of both the CMIP6 and CMIP5 ensembles are assessed by comparing the annual mean temperature changes and difference between summer mean temperature changes and winter mean temperature changes to multi-proxy Temperature 12k database (red, green; Kaufman et al., 2020b) and mean annual precipitation and difference between mean temperature of the warmest month (MTWA) changes and mean temperature of the coldest month (MTCO) changes to the pollen-based reconstructions (yellow, blue, purple; Bartlein et al., 2011). The better a model's changes fit with the reconstructions, then closer it should be to the green square (Taylor, 2001). The correlation coefficient is plotted on the azimuth, and the radial distance presents the ratio of the standard deviation in the model and reconstructions (after adjustment to account for the existence of uncertainty in them, Hargreaves et al., 2013).

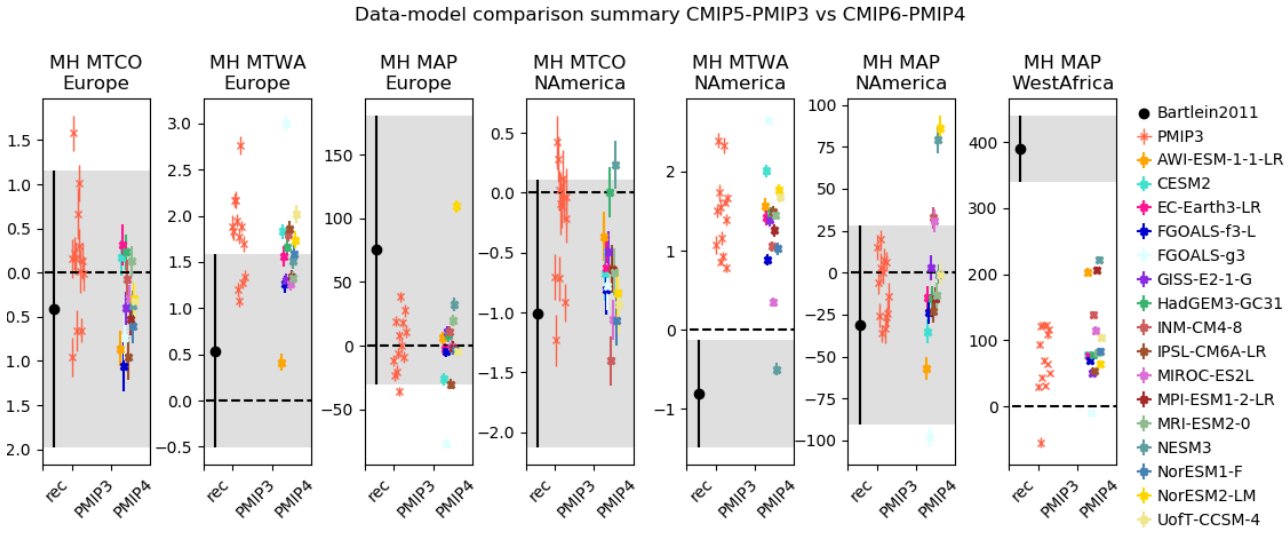

Figure S3. Alternate presentation of the data-model comparison. Regional comparisons using Monte-Carlo sampling of both the reconstruction uncertainty (Bartlein et al., 2011) and model uncertainty as expressed by variability of the 50-year-averaged climate change signal at individual proxy locations. The regions are defined as Europe (35–70°N, 10°W–30°E), West Africa (0–30°N,30°W–30°E) and North America (20–50°N,140–60°W).